Journal of Systems Engineering and Electronics
Vol. 37, No. 3, June 2026, pp.836 – 843

High isolation dual circularly polarized antenna in gap waveguide technology for mm-Wave satellite communications

QUAN Shuanglong[1,*], CAO Jianyin[1], HE Chao[1], and WANG Hao[1,2]

1. School of Electronic and Optical Engineering, Nanjing University of Science and Technology, Nanjing 210018, China;
2. Nanhu Laboratory, Jiaxing 314001, China

Abstract: A millimeter-wave (mm-Wave) dual circularly polarized (CP) antenna in gap waveguide (GWG) technology with high port isolation is proposed in this paper. It is consisted of a simplified orthomode transducer (OMT) and an improved multi-section hexagonal waveguide CP horn antenna. The OMT is composed of two metal layers without the traditional septum or iris, which makes the structure simpler. The CP horn antenna can be easily integrated with the OMT without mode conversion. The principle analysis as well as the simulated and measured results of the proposed antenna are given in this paper. The simulated and measured results agree very well with each other. The port isolation of more than 27 dB over bandwidth of 26.5–31 GHz ($|S_{11}|< -15$ dB) is achieved with relative bandwidth of 15.7%. The axial ratio (AR) lower than 2.5 dB for both left-hand and right-hand CP (LHCP and RHCP) are achieved over the bandwidth. The proposed antenna is a candidate for mm-Wave satellite communications or beyond fifth-generation (5G) communications applications.

Keywords: dual circularly polarized antennas, gap waveguide, orthomode transducer, millimeter wave.

DOI: 10.23919/JSEE.2025.000031

1. Introduction

In recent years, millimeter-wave (mm-Wave) frequency band is widely concerned due to its rich spectrum resources, small device size and high transmission rate. Recently, circularly polarized (CP) antennas with reduced polarization mismatch and resisted multipath effects have been developed for mm-Wave satellite communications. Dual CP antennas can further increase the system capacity by creating polarization diversity while maintaining a compact size [1,2]. Therefore, mm-Wave dual CP antennas have attracted great interest for researchers.

Manuscript received January 09, 2024.
*Corresponding author.
This work was supported by China Postdoctoral Foundation (2023M731680) and the Youth Foundation of Jiangsu Province (BK20230919).

Among the reported mm-Wave dual CP antennas, in addition to many types of planar side-fired antennas [3−9], the CP horn antenna in the form of end-fire is also widely used. It has the advantages of wide working frequency band, compact aperture, high radiation efficiency and easy processing. At present, the design methods of circular polarizer in this kind of antenna mainly include inserting metal or dielectric diaphragm in the waveguide [10,11], slotting in the waveguide [12−14], chamfering in the waveguide [15], loading ridge structure on the inner wall of the waveguide [16], inserting multiple groups of pins in the waveguide [17], using corrugated waveguide [18], using elliptical waveguide [19] and by loading various kinds of artificial hypersurfaces [20,21] or anisotropic lens structures [22,23] at the online polarization antenna terminals. In [24], a dual CP antenna with axial ratio (AR) lower than 3 dB and isolation greater than 15 dB from 17.6 GHz to 19.8 GHz (11.8%) is proposed based on substrate integrated waveguide (SIW). Similarly, a mm-Wave dual CP antenna with isolation greater than 10 dB was designed in [25]. The two antennas have compact profile, but the port isolation is high. At the same time, large errors will be generated in the processing of multi-layer structure, which limits the application of antenna in mm-Wave frequency bands. In [26], a dual CP antenna operating from 28.5 GHz to 31.2 GHz with isolation higher than 27 dB was proposed. Under similar design idea, a dual CP antenna was proposed in [27]. These two antennas are composed of a septum polarizer and a circular waveguide (CW) horn. However, the large size makes their application inconvenient in some fields, such as the reflector antenna feeder. In [28], a dual CP antenna with isolation greater than 15 dB and AR lower than 2.2 dB from 54 GHz to 60 GHz (10.5%) was proposed. The bandwidth of this antenna is not wide enough and its structure is complex. In [29], a dual CP antenna was designed with isolation greater than 22 dB and AR lower than 3 dB over the range of 50–75 GHz. In [30], a dual CP antenna was designed with isolation greater than 32.5 dB and AR lower than 2.8 dB from 80 GHz to 110 GHz by combining the grooved-wall CP horn and orthomode transducer (OMT). However, the structures of these two antennas are relatively complex and their sizes are relatively large.

In addition, as a component often used in the design of dual CP antennas, many kinds of OMTs have also been widely studied, such as onefold symmetry [31], twofold symmetry [32,33] and asymmetry OMTs [34]. In contrast, onefold and twofold symmetry OMTs need a power divider or a pair of ports for one polarization, which leads to the relatively complex structures.

Based on the above background, a mm-Wave high isolation dual CP horn antenna in gap waveguide (GWG) technology is proposed in this paper. Firstly, based on the traditional OMT, a novel and simple OMT is designed. It has a main arm directly fed to a WR-28 rectangular waveguide (RW) port for one polarization and a side arm for the other polarization. Then, a CP horn antenna based on multi-section hexagonal waveguide (HW) is constructed. The two parts are easy to combine due to no transfer mode conversion. In addition, the GWG is used for interconnection, so that the assembly does not need good electrical contact, which reduces the difficulty of antenna processing. Finally, the proposed antenna is simulated, processed and measured.

2. Antenna design

2.1 Antenna configuration

The geometry of the proposed antenna is shown in Fig. 1. The corresponding parameter values are listed in Table 1. The antenna consists of a T-shape OMT and a multi-section HW CP horn. Two WR-28 RW ports are adopted for the feeding. When Port 1 is fed, the polarization mode of the antenna is left-hand CP (LHCP), and when Port 2 is fed, the polarization mode is right-hand CP (RHCP). The antenna is designed as a tapered open horn shape to obtain good radiation characteristics.

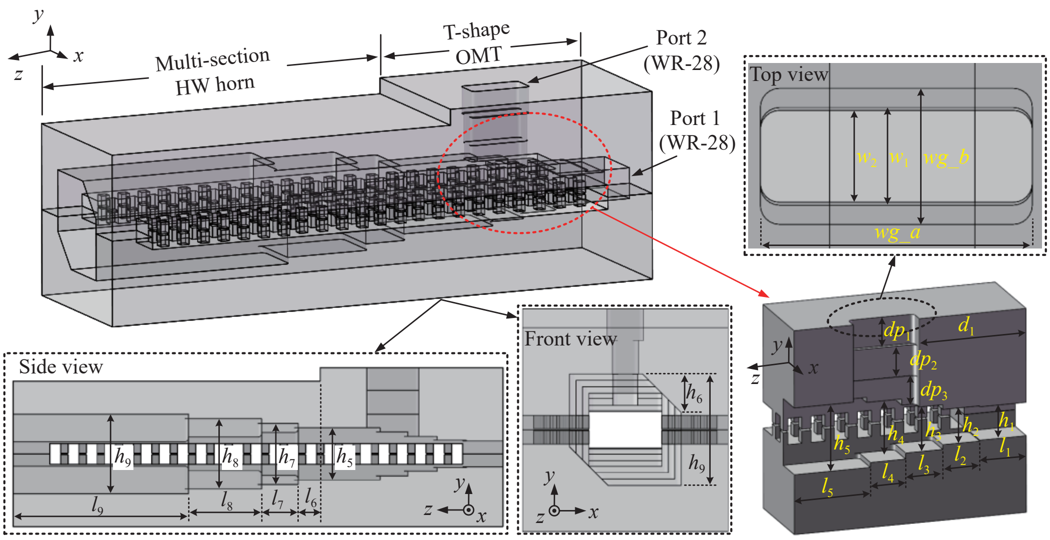

Fig. 1 Geometry of the proposed antenna

Table 1 Parameter list mm

Parameter	wg_a	wg_b	w_1	w_2	d_1	dp_1	dp_2	dp_3	h_1	h_2	h_3	h_4	h_5
Value	7.112	3.556	2.55	2.40	11.50	3.08	3.28	3.04	3.556	3.756	4.756	6.056	7.112
Parameter	h_6	h_7	h_8	h_9	l_1	l_2	l_3	l_4	l_5	l_6	l_7	l_8	l_9
Value	3.75	8.362	9.612	10.862	5.0	4.0	4.0	3.8	8.2	3.0	5.0	10.0	24.0

The section of T-shape OMT is shown in Fig. 1. It is fed by two RWs ports, and the output port is a square waveguide with side length of h_5=7.112 mm. Port 1 and Port 2 are standard RW WR-28 waveguide ports, which is conducive to the convenient interconnection between the antenna and other equipment or components without secondary interface conversion. This structure can be realized by vertically inserting a stepped RW above a RW port (Port 1) to square waveguide port. Generally, the insertion position is selected on the wide side midline to ensure the electric field of TE_{10} mode without been greatly affected. By optimizing the size of each part of the stepped structure, lower loss and higher port isolation can be obtained.

The structure of the multi-section HW CP horn is described in the side view and front view in Fig. 1. This part of the structure is fed by a square waveguide, and the side length of the square waveguide is equal to the square waveguide at the output port of the T-shape OMT. The HW structure is designed to realize the conversion from linear polarization to circular polarization. The multi-section stepped structure forms a radiator similar to the horn. Therefore, it is a combination of polarization converter and radiation horn.

In order to simplify the processing process and reduce the assembly difficulty, the antenna is divided into two layers and interconnected by GWG structure. The periodic arrangement of metal pin can achieve high impedance boundary conditions. The geometric shape and corresponding dispersion diagram of the periodic pin are shown in Fig. 2. The metal pins produce a frequency stop band of 22.6−53.5 GHz.

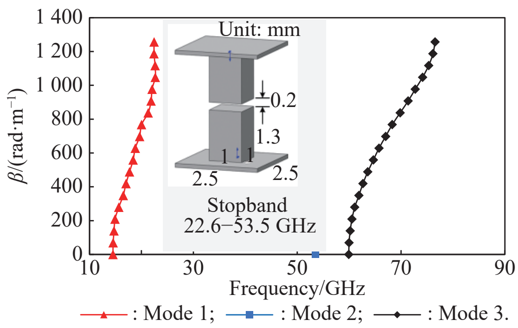

Fig. 2 Dispersion diagram of the periodic pin

2.2 OMT principle

The detailed structure and parameters of the OMT are shown in Fig. 1. The OMT can be treated as a four-port network, while the square waveguide port is a common port for both the horizontal polarization (HP) TE_{01} mode and the vertical polarization (VP) TE_{10} mode. Therefore, there is no need to convert the working mode between Port 1 and Port 3, or between Port 2 and Port 3. Thus, a good transition can be achieved. For the RW Port 1 and Port 2, high port isolation is also obtained, since the working mode of each other is cut-off under the size of the rectangular port. The *E*-field distribution of the HP TE10 mode and the VP TE01 mode on the symmetry plane is presented in Fig. 3. As can be seen, the horizontally polarized waves are directed to the lateral port, while the vertically polarized waves are guided to the axial port. At the same time, the isolation between the two RW ports (Port 1 and Port 2) is high.

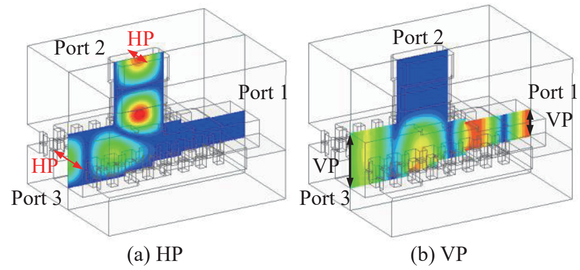

Fig. 3 *E*-field distribution on the symmetry plane of the OMT for HP and VP

As shown in Fig. 4, the proposed OMT is designed and simulated to verify the performance, by using high frequency electromagnetic simulation software ANSYS HFSS. The reflection coefficients for both polarizations are below −12.4 dB from 27 GHz to 31 GHz and a high isolation over 47 dB is achieved. A sudden increase in the return loss and insertion loss can be observed around 30 GHz which is caused by the excitation of the higher modes.

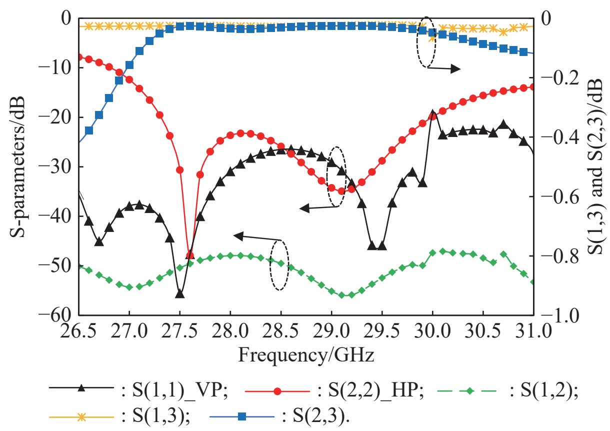

Fig. 4 Simulated results of the proposed OMT

2.3 Multi-section HW horn

The detailed structure of multi-section HW horn is also shown in Fig.1, and the corresponding size parameters are shown in Table 1. This design exploit differential dispersion in HW, which allows a linear to circular polarization conversion. To illuminate the operating principle of the proposed multi-section CP horn, the VP excited electric field for several sections of the horn are shown in Fig. 5. The electric field at the feed port is equivalent to two orthogonal components (E_1 and E_2). The phase shift constants β of E_1 and E_2 in HW transmission are different, which makes the phase of electromagnetic waves of the two modes different in the plane E. As shown in Fig. 6, the curves of β_1 and β_2 in three different sections of plane B, C and D are given.

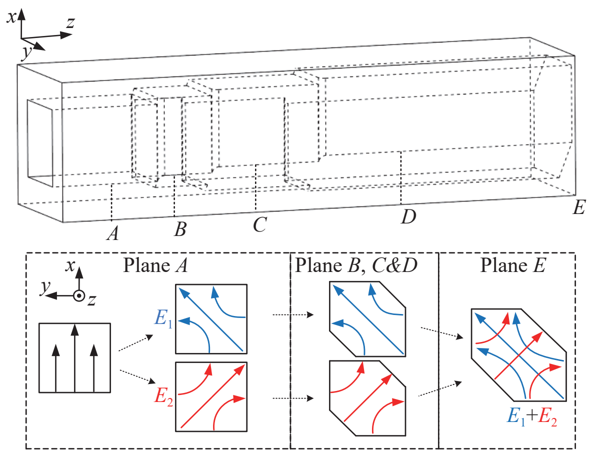

Fig. 5 Graph of electric field

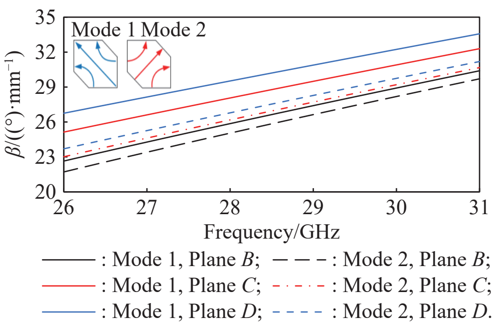

Fig. 6 Dispersion relations for several HWs

Thus, total phase lag between two modes in the plane E is given by

$$\begin{cases} \Delta\phi(f) = \Delta\phi_1(f) + \Delta\phi_2(f) + \Delta\phi_3(f) \\ \Delta\phi_1(f) = [\beta_{B2}(f) - \beta_{B1}(f)] \cdot l_7 \\ \Delta\phi_2(f) = [\beta_{C2}(f) - \beta_{C1}(f)] \cdot l_8 \\ \Delta\phi_3(f) = [\beta_{D2}(f) - \beta_{D1}(f)] \cdot l_9 \end{cases} . \quad (1)$$

By properly optimizing the size of multi-section HW CP horn, the phase difference can achieve around 90°, and the CP electromagnetic wave can be obtained.

The polarization mode of the horn is LHCP when excited by the VP mode. At the same time, the polarization mode of the horn is RHCP, when excited by the HP mode. The simulated AR of the proposed multi-section gap hexagonal waveguide CP horn are given in Fig. 7. In the range of 26.5−31 GHz, the simulated AR is lower than 1.8 dB for two polarization modes.

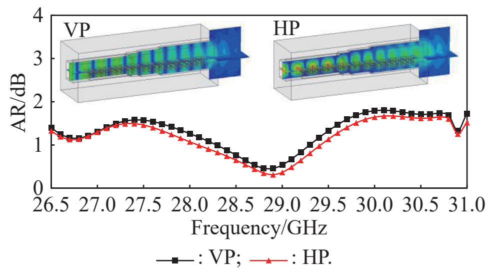

Fig. 7 Simulated AR results of the proposed CP horn

2.4 Design procedure

A simple stepwise proce dure for designing this proposed antenna is presented as follows.

Step 1 Based on the frequency requirements, determine the standard RW to feed the antenna.

Step 2 Design the OMT. Firstly, a transition structure from RW to square waveguide is designed, in which the side length of the square waveguide is equal to the wide side of the RW. Secondly, a stepped RW is inserted into the wide side midline of the transition structure. The feeding port of the stepped waveguide is a standard rectangular waveguide, and the wide side of the insertion port can be equal to the wide side of the standard RW, while the short side is slightly smaller. Adjust the size parameters of each transition structure, and optimize the performance of impedance matching and isolation.

Step 3 Design multi-section HW horn. The square waveguide of the previous step is used as the feed port. HW can be deformed by cutting off two right angles with square waveguide. The side length and waveguide length of each HW are the main variables to adjust and improve the working performance of the circular polarizer.

Step 4 Connect the two parts of the structure, divide the antenna structure according to the processing technology and use the gap structure for interconnection.

Step 5 Optimize the parameters of the model to meet the design requirements and complete the design.

3. Measurement and discussion

To verify the design, the dual-CP antenna is fabricated and tested. The fabricated sample of the proposed dual-CP antenna is shown in Fig. 8. All structural parts are made of aluminium alloy with computer numerical control (CNC) process. Photos of the antenna testing in an anechoic chamber is shown in Fig. 9.

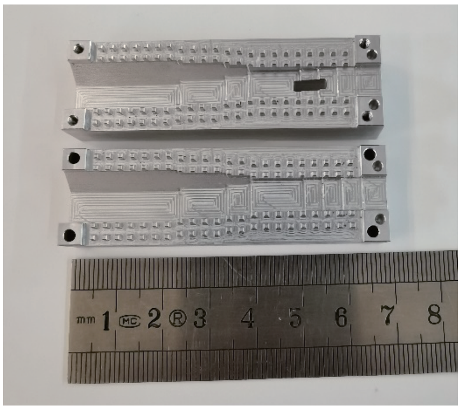

(a) Internal view

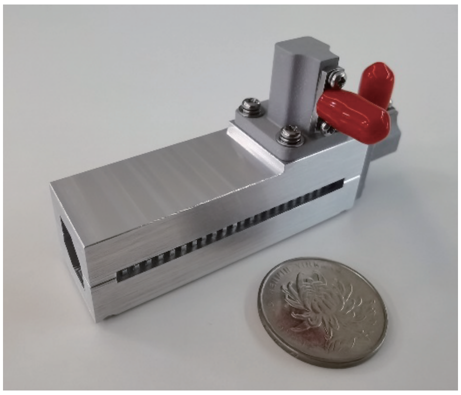

(b) Overall view

Fig. 8 Photo of the proposed dual CP antenna

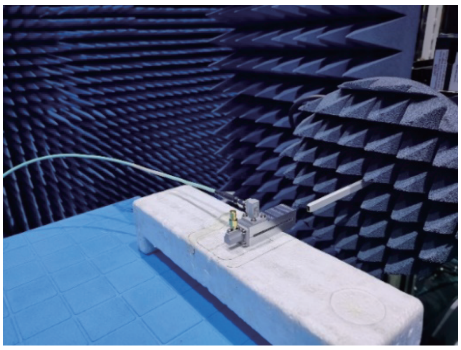

Fig. 9 Photo of antenna test

As shown in Fig. 10(a) and Fig. 10(b), the $|S_{11}|$ and $|S_{22}|$ of the antenna are simulated and measured for comparison. It can be noted that both the simulated and measured $|S_{11}|$ (<−15 dB), $|S_{22}|$ (<−15 dB) and $|S_{12}|$ (<−27 dB) are considerable in the range of 26.5 GHz to 31 GHz. The measured results of $|S_{22}|$ are basically consistent with the simulated results, while the comparison between the simulated and measured results of $|S_{11}|$ is not good, which is mainly caused by processing errors and assembly errors. However, the measured $|S_{11}|$ is generally below −15 dB, so it has little impact on the antenna performance. In addition, the measured results of $|S_{12}|$ are in good agreement with the simulated results.

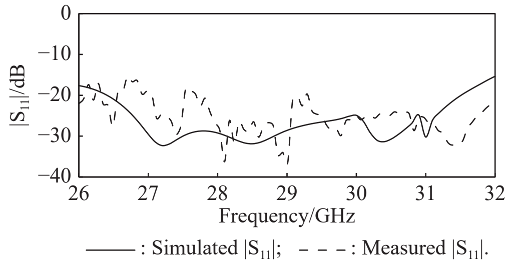

(a) $|S_{11}|$

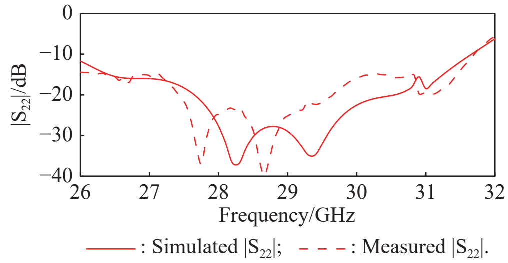

(b) $|S_{22}|$

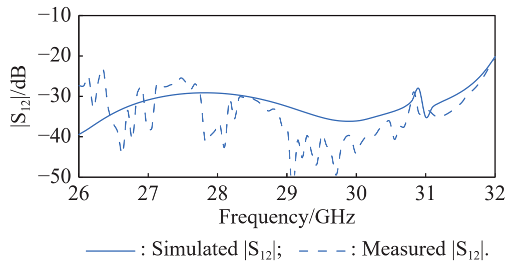

(c) $|S_{12}|$

Fig. 10 Simulated and measured results

The gain and AR frequency response curves of the antenna under two polarization conditions are presented in Fig. 11. The simulated peak LHCP and RHCP gain are 11.4 dBic and 11.5 dBic, respectively. The corresponding measured results are 10.9 dBic and 11.0 dBic, respectively. In addition, for LHCP port, the measured AR is less than 2.3 dB, and for RHCP port, the measured AR is less than 2.1 dB. The simulated and measured results of the dual CP antenna are in good agreement. Moreover, it is noted that fluctuations occur around 30.8 GHz. The phenomenon is caused by the excitation of the higher modes, the simulated and measured LHCP and RHCP radiation patterns and AR results of the proposed antenna at several typical frequencies in different planes (*x*-*z* plane and *y*-*z* plane) are shown in Fig. 12. The simulated and measured ARs are less than 3 dB in a wide beam range, which makes the proposed antenna suitable for the feed source/polarizer for high gain reflector antenna design. In addition, the measured main beam widths are in good agreement with simulations.

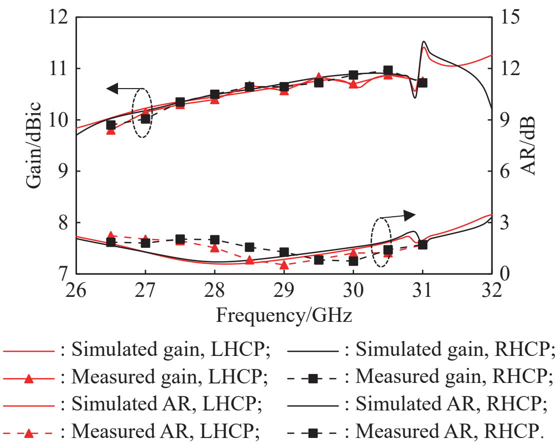

Fig. 11 Simulated and measured gains and ARs

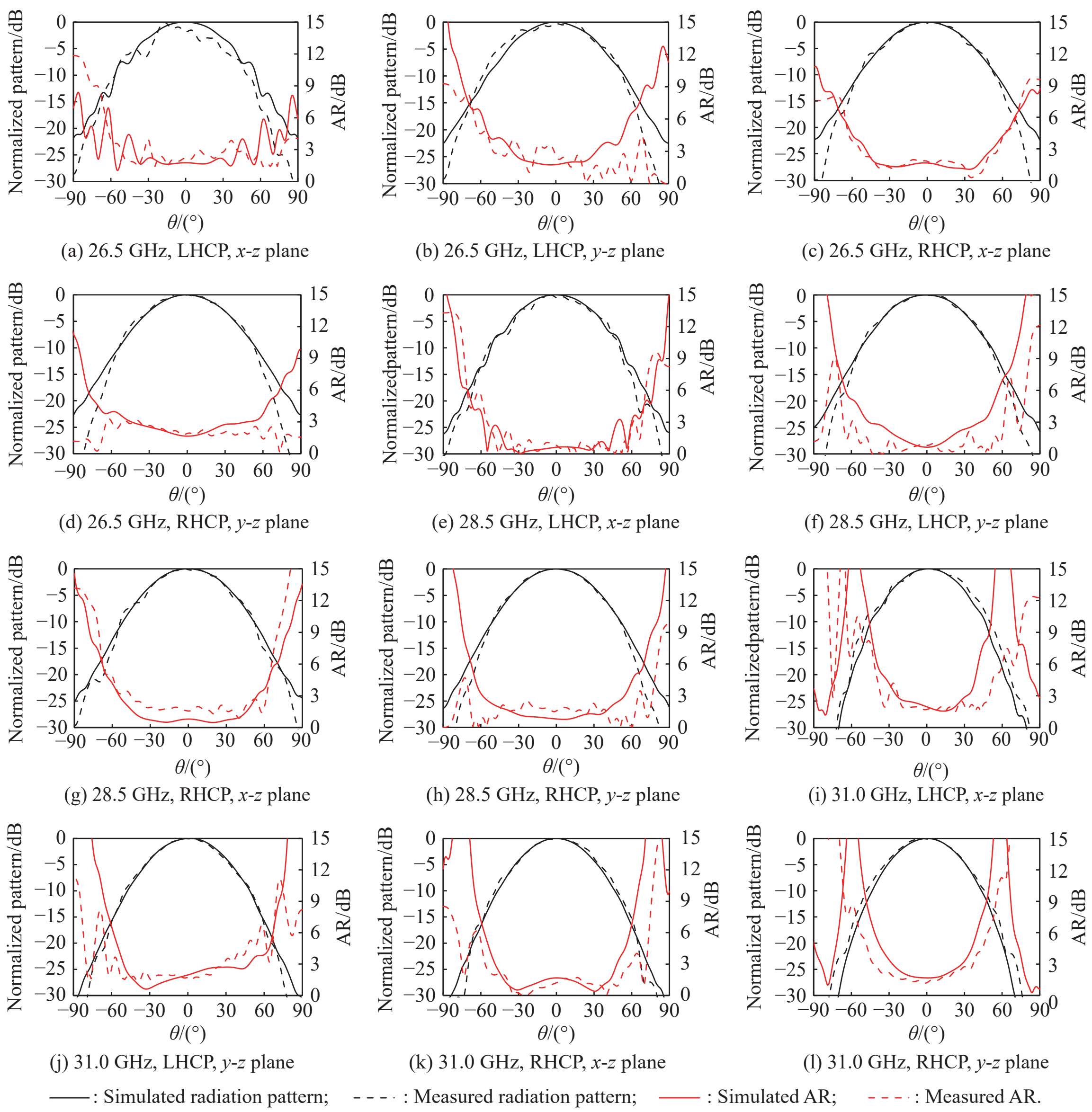

Fig. 12 Simulated and measured radiation pattern and AR results of the proposed dual-CP antenna

The performances between the antenna and previously reported dual CP antennas are compared in Table 2. It can be seen that the gain fluctuation of the proposed antenna is the lowest, even under the condition of the same relative bandwidth, which is more conducive to the use in broadband communication system. Compared with [24,26,28], the proposed design shows wider bandwidth and higher isolation. In [29,30], these two antennas achieve very wide bandwidth and high isolation, but their structures are more complex and their sizes are longer than those of the antenna proposed in this paper. In addition, compared with other transmission line types such as SIW [24], CW [26,28,30] and RW [29], the GWG technology is adopted to significantly reduce the assembly difficulty and cost, which makes the antenna more conducive for wide applications in the mm-Wave. Furthermore, the bandwidth of the proposed antenna is not particularly wide, just like the antenna in [29], which limits the application of the antenna in some systems requiring wider bandwidth.

Table 2 Performance comparison of several antennas

Method	Frequency/GHz	Reflection coefficient /dB	AR/dB	Isolation/dB	Overall bandwidth/%	Gain fluctuation/dB	Antenna length (λ_0)	Complexity	Technology
Method in [24]	17.6−19.8	< −13	< 3	⩾15	11.8	2.2	5.3	Simple	SIW
Method in [26]	28.5−31.2	< −25	−	> 27	9.0	−	12.5	Simple	CW
Method in [28]	54−60	< −10	< 2.2	> 15	10.5	−	≈ 8.1	Complex	CW
Method in [29]	50−75	< −13.8	< 3	> 22	37.4	6	≈ 8.8	Complex	RW
Method in [30]	80−110	< −20	< 2.8	> 32.5	31.6	4	21.6	Complex	CW
Proposed method	26.5−31	< −15	< 2.5	> 27	15.7	1.1	6.4	Simple	GWG

4. Conclusions

In this paper, a high isolation dual CP antenna composed of a simple OMT and a multi-section HW CP horn is designed in GWG technology. In the range of 26.5−31 GHz (15.7% relative bandwidth), the simulated and measured results agree very well. The port isolation larger than 27 dB is achieved with reflection coefficient lower than −15 dB and AR lower than 2.5 dB for both LHCP and RHCP. The measured gains for LHCP and RHCP are (10.35±0.55) dBic and (10.45±0.55) dBic respectively. The proposed antenna is suitable for mm-Wave satellite communications.

References

[1] ZHANG J, ZHAO K. Dual polarized phased array with endfire radiation for 5G handset applications. IEEE Trans. on Antennas and Propagation, 2020, 68(4): 3277–3282.

[2] QUAN S L, CAO J Y, HE C, et al. Millimeter-wave broadband dual-circularly polarized antenna based on gap waveguide technology. Journal of Systems Engineering and Electronics, 2024. DOI: 10.23919/JSEE.2024.000082.

[3] MAO C X, GAO S C. Compact broadband dual-sense circularly polarized microstrip antenna array with enhanced isolation. IEEE Trans. on Antennas and Propagation, 2017, 65(12): 7073–7082.

[4] LI J W, HU Y, XIANG L. Broadband circularly polarized magnetoelectric dipole antenna and array for K-band and Ka-band satellite communications. IEEE Trans. on Antennas and Propagation, 2022, 70(7): 5807–5912.

[5] YANG Y H, SUN B H, GUO J L. A low-cost single-layer dual circularly polarized antenna for millimeter-wave applications. IEEE Antennas and Wireless Propagation Letters, 2020, 18(4): 651–655.

[6] YUE T W, JIANG Z H, WERNER D H. A compact metasurface-enabled dual-band dual-circularly polarized antenna loaded with complementary split ring resonators. IEEE Trans. on Antennas and Propagation, 2019, 67(2): 794–803.

[7] ROCHER M F, HERRUZO J I H, NOGUEIRA A V. Dual-band single-layer slot array antenna fed by K/Ka-band dual-mode resonators in gap waveguide technology. IEEE Antennas and Wireless Propagation Letters, 2021, 20(3): 416–420.

[8] ZHU C M, XU G H, DING D W, et al. Low-profile wideband millimeter-wave circularly polarized antenna with hexagonal parasitic patches. IEEE Antennas and Wireless Propagation Letters, 2021, 20(9): 1651–1655.

[9] ZHU C M, XU G H, REN A D, et al. A compact dual-band dual-circularly polarized siw cavity-backed antenna array for millimeter-wave applications. IEEE Antennas and Wireless Propagation Letters, 2022, 21(8): 1572–1576.

[10] CHENG X H, YAO Y, HIROKAWA J, et al. Analysis and design of a wideband endfire circularly polarized septum antenna. IEEE Trans. on Antennas and Propagation, 2018, 66(11): 5783–5793.

[11] LI D Y, JIAO Y C, YU H W, et al. Wideband circularly polarized pyramidal horn antenna based on spoof surface plasmon polaritons. IEEE Trans. on Antennas and Propagation, 2021, 69(4): 2353–2358.

[12] MISHRA G, SHARMA S K, CHIEH J S. A circular polarized feed horn with inbuilt polarizer for offset reflector antenna for W-band cubesat applications. IEEE Trans. on Antennas and Propagation, 2019, 67(3): 1904–1909.

[13] AGNIHOTRI I, SHARMA S K. Design of a compact 3-D metal printed Ka-band waveguide polarizer. IEEE Antennas Wireless Propagation Letters, 2019, 18(12): 2726–2730.

[14] REN Q N, ZAMAN A U, YANG J. Dual-circularly polarized array antenna based on gap waveguide utilizing double-grooved circular waveguide polarizer. IEEE Trans. on Antennas and Propagation, 2022, 70(11): 10436–10444.

[15] BHARDWAJ S, VOLAKIS J L. Hexagonal waveguide based circularly polarized horn antennas for Sub-mm-Wave/Terahertz band. IEEE Trans. on Antennas and Propagation, 2018, 66(7): 3366–3374.

[16] LU K, LEUNG K W, YANG N. 3-D-printed circularly polarized Twisted-Ridge horn antenna. IEEE Trans. on Antennas

and Propagation, 2021, 69(3): 1746–1750.
[17] SUBBARAO B, FUSCO V F. Compact coaxial-fed CP polarizer. IEEE Antennas Wireless Propagation Letters, 2004, 3: 145–147.
[18] ROY S S, NAGASEKHAR T, SAHA C, et al. Dual band (S-X) ground station antenna for low Earth orbit (LEO) satellite tracking application. IEEE Access, 2022, 10: 80910−80917.
[19] YU H Y, YU J S, LIU X M, et al. A wideband circularly polarized horn antenna with a tapered elliptical waveguide polarizer. IEEE Trans. on Antennas and Propagation, 2019, 67(6): 3695–3703.
[20] LIN C X, GE Y H, BIRD T S, et al. Circularly polarized horns based on standard horns and a metasurface polarizer. IEEE Antennas Wireless Propagation Letters, 2018, 17(3): 480–484.
[21] CHANG X, WANG H B, LI T J, et al. Shared-aperture phased array antenna with codesigned near-field coupled circular polarizer loaded for K/Ka-band wide-angle satellite communication. IEEE Trans. on Antennas and Propagation, 2022, 70(9): 7478–7490.
[22] DING C, LUK K M. Wideband high-gain circularly polarized antenna using artificial anisotropic polarizer. IEEE Trans. on Antennas and Propagation, 2019, 67(10): 6645–6649.
[23] ZHANG Y X, JIAO Y C, ZHANG L. Wideband inhomogeneous-polarizer loaded circularly polarized SIW horn antenna for broadband millimeter-wave applications. IEEE Antennas Wireless Propagation Letters, 2019, 18(7): 1448–1452.
[24] CAI Y, ZHANG Y S, QIAN Z P, et al. Compact wideband dual circularly polarized substrate integrated waveguide horn antenna. IEEE Trans. on Antennas and Propagation, 2017, 64(7): 3184–3189.
[25] WU Q, HIROKAWA J, YIN J X, et al. Millimeter-wave multibeam endfire dual-circularly polarized antenna array for 5G wireless applications. IEEE Trans. on Antennas and Propagation, 2018, 66(9): 4930–4935.
[26] ADDAMO G, PEVERINI O A, MANFREDI D, et al, Additive manufacturing of Ka-band dual-polarization waveguide componentsIEEE Trans. on Microwave Theory and Techniques, 2018, 66(8): 3589–3596.
[27] SHU C, WANG J B, HU S Q, et al. A wideband dual-circular-polarization horn antenna for mmWave wireless communications. IEEE Antennas and Wireless Propagation Letters, 2019, 18(9): 1726–1730.
[28] LUO N N, YU X H, MISHRA G, et al. A millimeter-wave (V-band) dual-circular polarized horn antenna based on an inbuilt monogroove polarizer. IEEE Antennas and Wireless Propagation Letters, 2020, 19(11): 1933–1937.
[29] CHENG X H, YAO Y, YU T, et al. Wideband dual circularly polarized antipodal septum antenna for millimeter wave applications. IEEE Trans. on Antennas and Propagation, 2021, 69(6): 3549–3554.
[30] SHU C, HU S Q, CHENG X H, et al. Wideband dual-circular-polarization antenna with high isolation for millimeter-wave wireless communications. IEEE Trans. on Antennas and Propagation, 2022, 70(3): 1750–1763.
[31] ABDELAAL M A, SHAMS S I, MOHARRAM M A, et al. Compact full band OMT based on dual-mode doubleridge waveguide. IEEE Trans. on Microwave Theory Technology, 2018, 66(6): 2767–2774.
[32] RUIZ-CRUZ J A, MONTEJO-GARAI J R, LEAL-SEVILLANO C A, et al. Orthomode transducers with folded double-symmetry junctions for broadband and compact antenna feeds. IEEE Trans. on Antennas and Propagation, 2018, 66(3): 1160–1168.
[33] ABDELAAL M A, KISH A. A K-band 3-D-printed wideband groove gap waveguide orthomode transducer. IEEE Trans. on Microwave Theory Technology, 2019, 67(8): 3361–3369.
[34] SAEIDI-MANESH H, SAEEDI S, MIRMOZAFARI M, et al. Design and fabrication of orthogonal-mode transducer using 3-D printing technology. IEEE Antennas and Wireless Propagation Letters, 2018, 17(11): 2013–2016.